Materials Research Express

PAPER

A first-principles study of magnetic properties of $Zn_{0.94}Mg_{0.01}Mn_{0.05}O$

IOP Publishing Mater. Res. Express 6 (2019) 126118 https://doi.org/10.1088/2053-1591/ab63f6

Materials Research Express

RECEIVED
30 September 2019

REVISED
6 December 2019

ACCEPTED FOR PUBLICATION
19 December 2019

PUBLISHED
10 January 2020

PAPER

A first-principles study of magnetic properties of $Zn_{0.94}Mg_{0.01}Mn_{0.05}O$

I P Duru[1], E Ozugurlu[2] and L Arda[3,4]

[1] Marmara University, Department of Physics, Faculty of Science and Literature, 34722, Kadikoy, Istanbul, Turkey
[2] Istanbul Technical University, Department of Mathematics, 34469, Istanbul, Turkey
[3] Bahcesehir University, Faculty of Engineering and Natural Sciences, Department of Mechatronic Engineering, 34349, Besiktas, Istanbul, Turkey
[4] Author to whom any correspondence should be addressed.

E-mail: lutfi.arda@eng.bau.edu.tr

Keywords: Mg/Mn-doped ZnO, first-principles study, density functional theory, GGA + PBE, Monte Carlo methods, room temperature ferromagnetism

Abstract

The structural and magnetic properties of Mg/Mn-doped ZnO were investigated by the first-principles study and Monte Carlo methods (MCs). Applying magnetic force theorem (MFT) and using Kohn-Sham orbitals in the GGA-PBE scheme, the exchange coupling parameters (J) were calculated to figure out the magnetic interactions between atomic sites. Mn-Mg volume clustered (C1) ferromagnetic (FM) state was preferred; herewith, the calculated magnetic moment of Mn was 4.19μ_B and Mg has the highest moment value when clustered with Mn ions. Nearest Mn ions interacted antiferromagnetic (AFM) despite the increasing distance lead them to be in FM. However, AFM/FM wasoriginated from the p-d hybridization, superexchange interaction and direct exchange between distant Mn ions. In addition, the Curie temperature (T_c) was calculated as 311K using averaged magnetization and magnetic susceptibility via MC.

1. Introduction

Zinc oxide (ZnO) has become an important semiconductor material with a wide direct band gap of 3.37 eV and a large exciton binding energy of 60 meV at room temperature [1–17]. ZnO crystal with wurtzite geometry is an II–VI compound semiconductor [18, 19]. These features make it broadly useful in optoelectronic devicesand photoelectric applications, namely,gas sensors, transparent conductive oxides, and light-emitting devices [19–22]. In this perspective, metal oxides are particularly favorable materials used in primary technologies such as photovoltaics or solar fuel production as well as in energy storage technologies (e.g. batteries) [6, 13]. Besides, ZnO can be turned into a diluted magnetic semiconductor (DMS) via doping certain concentrations of impurity atoms, especially transition metals, and gain significant magnetic properties. Ferromagnetism (FM) at room temperature (RT) provides a wide area for device applications [11, 12, 14, 15, 23–25]. Since FM behavior almost induced by structural and electronic properties of a material (also ZnO), previous and latest theoretical studies focused on these features to investigate the origin of magnetism and interested properties. Xue *et al* found that Ni-3d and O-2p states had a strong hybridization near Fermi level in Ni-doped zinc blende (ZB) ZnO and magnetic moments mainly originated from the unpaired Ni 3d orbitals, and the O 2p orbitals contribute a little to the magnetic moments [26]. Khalid *et al* [11] observed shifting of Fermi level in the conduction band with increasing metal concentrations and metal-doped ZnO having ferromagnetic naturevia DFT with generalized gradient approximation (GGA). Moreover, Fedorov *et al* [12] reported ferromagnetism induced by intrinsic defects in ZnO (DFT-GGA). Mamamouni *et al* [14] focused on the electronic structure of the V-doped ZnO system using DFT resulting in Ruderman–Kittel–Kasuya–Yosida (RKKY)interaction and the atomic spin polarization of V were the key factors for the presence of ferromagnetism in V-doped ZnO system. However, at room temperature, particle size sensitive ferromagnetism was observed for ZnO nanoparticlesand oxygen

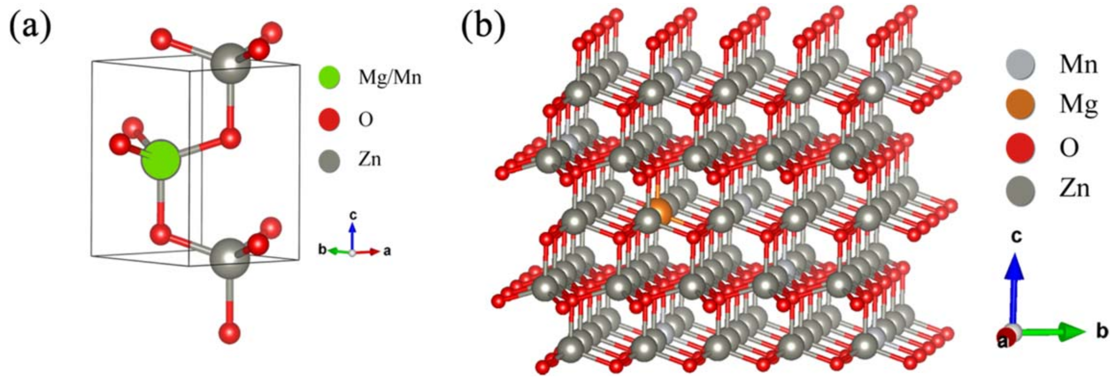

Figure 1. (a) Unit cell (b) Supercell of hexagonal ZnO.

vacancies playedacrucial role inthe size of the nanoparticles [15]. Cao *et al* [23] interested inthe electronic and magnetic properties of (Mn,Fe)co-doped ZnO within the GGA and GGA + U schemes resulting in aground state ferromagnetic ordering, which was mediated by double exchange mechanism. Electronic and magnetic properties of the Mn-doped ZnO semiconductor were calculated by the full-potential linearized augmented plane wave (FP-LAPW) method with the local spin density approximation (LSDA) and the modified Becke–Johnson (mBJ) potentialconsidering magnetic interaction between the Mn atoms, both the near and far positions exist [24]. Recently, El Haimeur *et al* [25] investigated the optical, electronic, and magnetic properties (Curie temperature, magnetic moment) of $Zn_{1-x}M_xO$ (M = Fe 5%, Co 1%, Cr 5%, and Mn 5%) by KKR method and deduced that TM impurities induce ferromagnetism with the Curie temperature closer to roomtemperature. In contrast, Liu *et al* [27] reported that Mn-doped ZnO exhibited antiferromagnetism, only Co-Mnco-dopedZnO possessed high Tc of better ferromagnetism rather than Co or Mn-doped ZnO. Gallegos *et al* [28] showed that magnetic moment lowered by the presence of oxygen vacancies, which could lead to a phase transition from FM to AFM. According to Goumrhar *et al* [29], 6% Mn doping caused ferromagnetic behavior, which was originated from double exchange interaction, p-d hybridization. On the other hand, Mg doping to ZnO increased bandgap [30–32]. Singh and Chae [33] showed that nanoparticles of MgO exhibited ferromagnetism and improved optical and dielectric behavior. Chen *et al* [34] showed that under external electric field, was used to tune magnitude of band gap and band dispersion, ZnMgO monolayer isa direct band gap semiconductor [30]. Özgür *et al* [4] calculated the band gap of ZnMgO as 3.37 eV and showed that their results were consistent with the experimental results.

Present work presents a relatively wide content focused on the magnetic properties through structural analysis of $Zn_{0.94}Mg_{0.01}Mn_{0.05}O$ based on the experimental data. Structural information and magnetic moments of four distinct distributions of dopants (Mg/Mn) as surface cluster (L1)/surface non-cluster (L2), volume cluster (C1), and volume non-cluster (C2) were obtained by performing density functional theory calculations (DFT) with the generalized gradient approximation (GGA) in the Perdew-Burke-Ernzerhof (PBE) scheme. The magnetic force theorem (MFT) was used to calculate exchange couplings J, between atoms in lattice sites. Thus, the most favored magnetic state was determined and the origin of magnetism was revealed. Finally, a fastened procedure was applied to calculate the Curie temperature (T_c) by Monte Carlo methods based on the Metropolis algorithm since RT ferromagnetism was demanded materials.

1.1. Computational details

The effects of dopant concentration and site positioning of impurity ions to magnetic behavior were determined by performing first-principles calculations using the OpenMx 3.8 package [35]. Two main modes, namely, volume and surface cases, were devised to modestly specify the most preferable formation of doped structure. Such an exertion would provide essential information about the distribution tendency of the impurity atoms either layered or cubed. Besides, the nearest neighboring of Mn ions as clusters point out the Mn-O-Mn bonding while only Zn-O-Mn bonding should be apparent for the parted Mn ions. Previous studies showed that clustering of doped atom is preferable in contrast to unclustered/randomly distributions (for ZnNiO [36–41]; for ZnMnO [24, 27–29, 42–47]; for ZnMgO [4, 30–34, 40, 48]; for ZnCrO [25, 49]; for ZnCoO [27, 29, 37, 47, 50]) even though it is not sufficiently evident for Mg/Mn doped ZnO such a low concentration of dopants. Hence, Mg was incorporated into the ZnMnO for both cases such as closest and distant to Mn ions clusters.

Geometry optimizedatomic positions were initially assigned for both antiferromagnetic (AFM) and ferromagnetic (FM) states of spin-polarized energy calculation via solving Kohn-Sham equations using plane-wave pseudopotentials and pseudoatomic orbitals briefly PAOs basis functions of Zn, Mn, Mg and O [51–54].

GGA was used in the Perdew-Burke-Ernzerhof (PBE) [55] scheme for exchange-correlation function assigning SCF criteria as 1.0E-7 Ha and k-points has been set to 12 × 12 × 4 for Monkhorst-Pack grid [56] restricting the energy range of density of states between −20 and 20 eV. However, AFM and FM phases were investigated dealing with collinear spins along c direction neglecting spin-orbit interaction due to its trivial contribution to the current structure. We determined exchange coupling constants, J_{ij}, between strongly localized moments of different atomic sites by a magnetic force theorem [57] since total energy could not be known in advance. For a better magnetic characterization of many-particle systems, Heisenberg model can be used with predetermined exchange coupling constants which can be obtained via DFT calculations. Lack of direct experimental measurement, in particular, to determine these parameters, several approaches took place [58–62] and one of them was based on LDA through magnetic phase states (MTS) which were detailed by Zeng *et al* [58] in a theoretical manner. Boukhvalov *et al* [59] reported a Hubbard correction (U) included the LDA method, namely, LDA + U to handle Heisenberg exchange coupling parameters (J) more realistic. They calculated effective J parameters for Mn clusters. A Green's function formalism was developed in order to be applicable to a non-orthogonal basis set, on account of a better estimation of exchange couplings. Equation (1), which was arisen from rigid spin approximation (RSA) applied to DFT ground state [42–45], was used to calculate J_{ij} between i and j sites where Gij denotes the Kohn-Sham orbital states related spin-dependent single-particle Green's function, and V_{ij} is the exchange interaction potential [63].

$$J_{ij} = \frac{1}{2\pi}\int^{\varepsilon F} d\varepsilon \; Tr[\hat{G}_{ij}^{\uparrow} \hat{V}_j \hat{G}_{ji}^{\downarrow} \hat{V}_i] \tag{1}$$

2. Results and discussions

ZnMgMnO supercell ($P6_3mc$ space group) was constructed based on experimental lattice parameters (given in table 1) via packaging 5 × 5 × 2 of the ZnO unit cell having totally 200 atoms. Mn and Mg concentrations were fixed to 5% and 1%, respectively during simulations. Composition with optimized Mn/Mg positions in hexagonalstructure to total energies was also given in table 1 and figure 1. L1, L2, C1, and C2 are labels set to represent cluster/non-cluster surface layers and cubed volume distributions. Only Mn cluster with Mg cluster/non-cluster distribution was adequately built to investigate the electronic and magnetic properties due to a common assent, which suggested that the behavior of dopant ions was clustering in a host material. The energy difference $\Delta E = E_{AFM}$-E_{FM} of these structures indicates that the favorable magnetic phases are either ferromagnetic (FM) or antiferromagnetic (AFM). $(\Delta E)_{L1} = 1.947$ meV and $(\Delta E)_{L2} = 4.60$ meV refer to an FM ground state for both surface layered distributions; herewith, non-clustered Mg possessed a bigger energy difference. In C1 and C2 cases, $(\Delta E)_{C1}$ and $(\Delta E)_{C2}$ were found to be 11.6 meV and 6.5 meV, respectively. Note that ΔE of volume distributions was higher than surface ones; in fact, volume clustering had the highest value comparing with the rest of the studied distributions. In addition, since physical properties are mostly related to structural content, bond angles and bond lengths were calculated by a self-coded script importing geometry optimized L1, L2, C1, and C2 crystallographic data (see tables 2 and 3).

According to table 2, the closest connection was observed between Mn and O ions through geometryoptimizedsupercell. In addition, other Mg-O and Zn-O couples inherently came close to each other rather than other couples such as Mn-Mn, Zn-Mn. For instance, Mn-Mn possessed far more distance directly related to Mn-O couples getting close. Besides, experimental bond length [64] had the best fit for Mg-O bond length in L2 (1.952317 Å) distributionin which Mg occupied the most distant location to the Mn cluster.

Bond angles and standard deviation of optimized geometries were calculated by averaging angles for each species existing in ZnMgMnO the structure including standard deviation per means of bond angles. The interdependency of these angles and lengths determines the variety of the exchange interactions, both directly and indirectly, due to the electronic occupancy of atomic orbitals. Thus, the hybridizing of certain ones (p-d) should control the atomic magnetic behavior of the system that is induced by the structural properties of materials like bond angles. According to table 3, label (2) and label (8) bond angles did not exist in the L2 and C2 distributions due to the distant position. Even though, one does not have a piece of exact information, in which atoms make certain bonds to dramatically contribute tothe magnetic phase of the system. Indirect exchange mechanisms, in particular, superexchange and double exchange determining magnetic behavior, ferromagnetic or antiferromagnetic, naturally occurred through A-O-B like triple bounded via oxygen (A and B should be the different ion of the same atom or totally different atoms) [65–67].

Averaged bond angles were shown in figure 2 with standard deviation. In non-clustered distributions, whole angle values of L2 and C2 practically overlap except O-Mn-O; on the contrary, bond angles of L1 and C1 are mostly different from each other except O-Zn-O and Zn-O-Zn. These triples possessed very close values for all distributions, most probably, according to the low dopant concentration and clustered Mn ions. Figure 3

Table 1. Dopant distribution and lattice parameters with corresponding energies of 5% Mn and 1% Mg-doped ZnO. Cluster and non-cluster emphasize the absolute location of the Mg atom. Mn and Mg atoms were represented by purple and orange spheres respectively; meanwhile, it was preferred to illustrate Zn and O by gray and red sticks. Experimental lattice parameters (a = 3.237 (Å), c = 5.195 (Å)) were obtained from [64].

Superlattice	Dopant Dist.	Label	ΔE/p.a. (meV)	Type
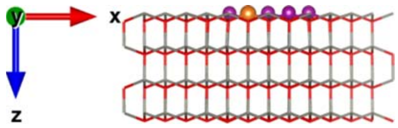	Cluster (Layer)	L1	1.947	FM
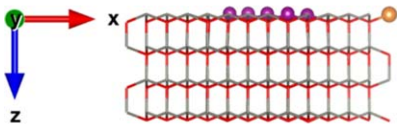	Non-Cluster (Layer)	L2	4.60	FM
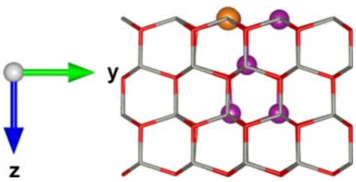	Cluster (Cubed)	C1	11.6	FM
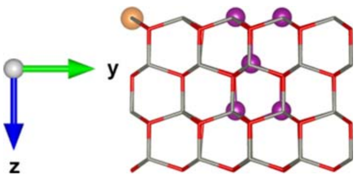	Non-Cluster (Cubed)	C2	6.5	FM

Table 2. Bond lengths (Å) of surface/volume cluster/non-cluster 5% Mn and 1% Mg doped ZnO. Cluster and non-cluster emphasize the absolute location of the Mg atom where experimental bond length of Zn/Mg/Mn-O is 1.9751Å.

A-B	L1	L2	C1	C2
Mn-O	1.830803	1.832177	1.806310	1.818967
Mn-Mn	2.912766	2.881406	2.956275	2.948955
Mn-Zn	3.173357	3.081449	3.129474	3.130044
Zn-O	1.933964	1.928778	1.929200	1.935550
Mg-Mn	3.200071	8.724499	3.174350	11.411750
Mg-O	1.940216	1.952317	1.930428	1.947546
Mg-Zn	3.193412	3.168307	3.172892	3.161646
Zn-Zn	3.157933	3.161942	3.157375	3.152024
O-O	3.034565	3.056118	2.997663	2.997219

illustrates the A-C bond length corresponding to the A-B-C bond angle with a linear fit. Note that variation in bond angle may not affect the bond length of any third-part atom which is bounded to B. As shown in figure 3, one can deduce that existence of Mn ions distinguishably reduces not only reduce bond angles and bond lengths but also lead to Mn-Mn direct coupling (see Mn-O-Mn and O-Mn-O data). However, other couplings and bonds including also Mg can be seen as a part of a fingerprint-like distribution that forms the 'spinal' of the system; besides, L1, C1 and L2, C2 resemble each other.

Orbital and total magnetic moments were obtained in terms of μB from spin-polarized DFT calculations point out the effect of clustering and non-clustering configurations even surface and volume type. In case of C1, the magnetic moment of Mn, Mg, Zn, and O were found to be 4.197248666 μB, 0.020923716 μB, 0.003242702 μB, and 0.017441612 μB, where Mn is the main contributor mostly from all five d-orbitals that almost possessed equal values. Similar results were obtained from other configurations. Mg of C1 or L1

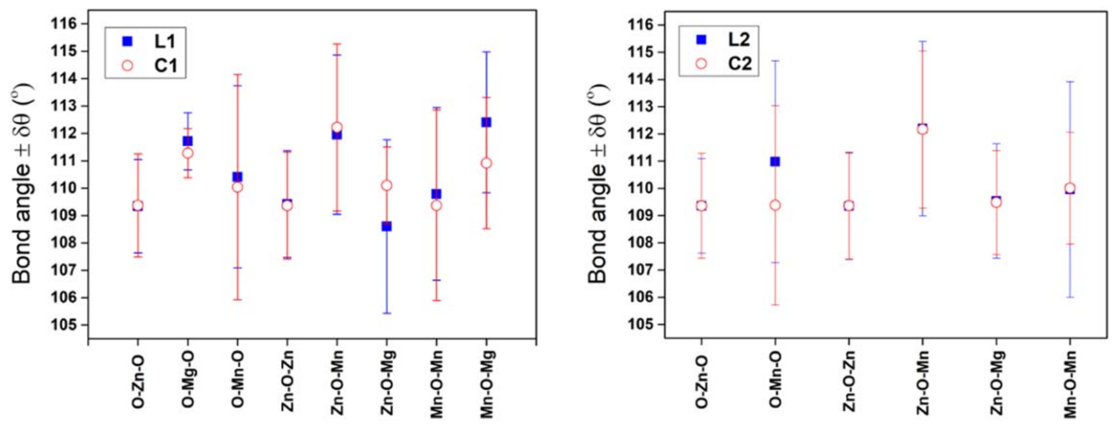

Figure 2. Average bond angles with a standard deviation of L1/C1 and L2/C2 distributions.

Table 3. Averaged bond angles ($\bar{\theta}$), standard deviations ($\delta\theta$) and standard deviation per mean of bond angle $\delta\theta/\bar{\theta}$ of surface/volume cluster/non-cluster 5% Mn and 1% Mg doped ZnO. Cluster and non-cluster emphasize the absolute location of the Mg atom.

A-B-C		L1(°)	L2(°)	C1(°)	C2(°)
O-Zn-O (1)		109.3403	109.3593	109.3679	109.3623
O-Mg-O (2)		111.7121	—	111.2767	—
O-Mn-O (3)		110.4099	110.9802	110.0351	109.3771
Zn-O-Zn (4)		109.4175	109.3459	109.3604	109.3669
Zn-O-Mn (5)		111.9530	112.1984	112.217	112.1668
Zn-O-Mg (6)		108.5981	109.5376	110.1002	109.4825
Mn-O-Mn (7)		109.7866	109.9598	109.3726	110.0091
Mn-O-Mg (8)		112.4028	—	110.9134	—
Standard deviation ($\delta\theta$) –Standard deviation per average bond angle $\delta\theta/\bar{\theta}$					
1	$\delta\theta$	1.7083	1.7410	1.88305	1.9309
	$\delta\theta/\bar{\theta}$	0.0156	0.0159	0.0172	0.0177
2	$\delta\theta$	1.0439	—	0.89422	—
	$\delta\theta/\bar{\theta}$	0.0093	—	0.008	—
3	$\delta\theta$	3.3258	3.7128	4.11764	3.6634
	$\delta\theta/\bar{\theta}$	0.0301	0.0335	0.0374	0.0335
4	$\delta\theta$	1.9521	1.9577	1.95381	1.9655
	$\delta\theta/\bar{\theta}$	0.0178	0.0179	0.0179	0.0180
5	$\delta\theta$	2.9075	3.2011	3.0474	2.8824
	$\delta\theta/\bar{\theta}$	0.026	0.0285	0.0272	0.0257
6	$\delta\theta$	3.1714	2.1002	1.40245	1.906
	$\delta\theta/\bar{\theta}$	0.0292	0.0192	0.0127	0.0174
7	$\delta\theta$	3.1539	3.9608	3.48413	2.0490
	$\delta\theta/\bar{\theta}$	0.0287	0.0360	0.0319	0.0186
8	$\delta\theta$	2.573	—	2.3956	—
	$\delta\theta/\bar{\theta}$	0.0229	—	0.0216	—

configurations had larger magnetic moments than C2 or L2 configurations. Moreover, not only Mn moment values were lowest for clustered structures but also Mn in C1 possessed the lowest value. In addition, magnetic moments are in agreement with the experimental findings of nanoparticles [23, 25, 27, and 68]. As a secondary dopant and an eligible band-gap tuner, Mg ion also affected the strength of the magnetic state when its location changed; on the other hand, magnetic moment differed according to the distance of Mg-Mn pairs (figure 4).

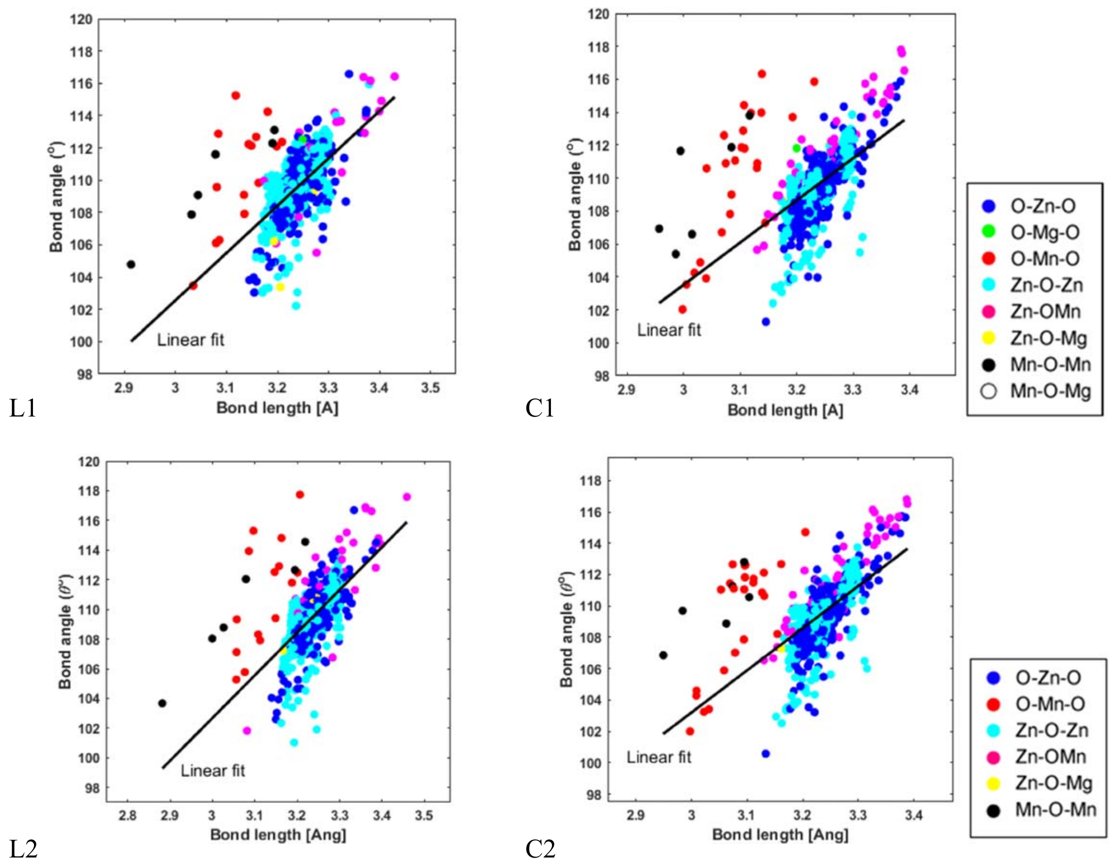

Figure 3. Bond angles—bond length (fingerprint) of surface/volume cluster/non-cluster 5% Mn and 1% Mg doped ZnO. Cluster and non-cluster emphasize the absolute location of the Mg atom.

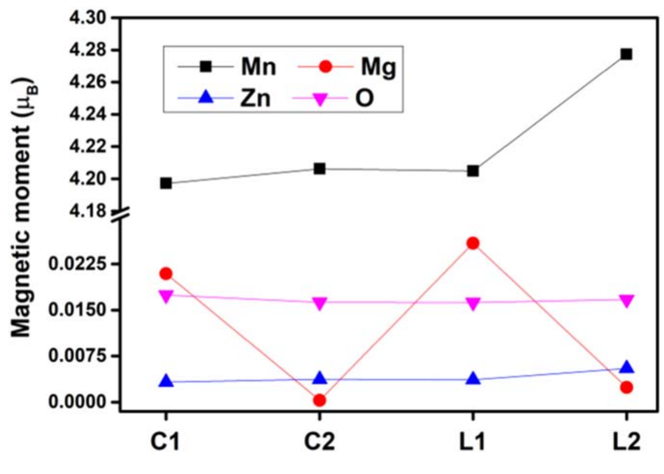

Figure 4. Magnetic moments of host and guest atoms for C1, C2, L1 and L2 states of 5% Mn and 1%Mg doped ZnO.

Further magnetic properties were investigated via calculating J exchange coupling constants between host and guest atoms to reveal direct and indirect exchange interactions, especially superexchange, double-exchange, and orbital hybridizations which lead the material gain ferromagnetic (including ferrimagnetism) behavior because of impurity atoms. Since C1 possessed the most stable ferromagnetism, we calculated J values only for this state. Bond lengths, the sign of exchange interaction (AFM/FM), and J values aregiven in table 4. Besides, detailed information on distance and neighboring oxygen type reveals the correlation between structural property and magnetic behavior; in fact, orbital hybridizations and indirect mechanisms should be appropriately explained. One can remember that there are 5 Mn atoms in which 4 of them were located around an Mn atom in cubed volume configuration. 2.99412 Å and 2.98579 Å distant Mn-Mn pairs showed strong AFM

Table 4. Bond length (Å), exchange couplings J (meV) and interaction type of C1 state of 5% Mn and 1% Mg doped ZnO. [a]Mn neighboring oxygen, [b,c]Zn neighboring oxygen, [d]Mn neighboring Mn, [e,f]Zn neighboring oxygen, [g]Mn neighboring Mg.

A-B	Bond length (Å)	Bond angle (°)	J (meV)	Exchange interaction
Mg-O[a]	2.03695	—	−0.64512	AFM
Mg-O[b,c]	1.93301[b], 1.93029[b]	—	−0,6E-3[b]	AFM
Mn[d]-O[a]	1.80631	—	4.4241	FM
Mn[d]-O[e,f]	1.93042[d], 1.88709[d]	—	2.2062[d], 3.3441[d]	FM
Mn[d]-Mn[d]	2.99412	111.6516	−21.7587	AFM
Mn[d]-Mn[d]	5.09671	175.6310	−3.82155	AFM
Mn[d]-Mn[d]	2.98579	105.3924	−25.9286	AFM
Mn[d]-Mn[d]	5.07144	176.7154	−4.12166	AFM
Mn[d]-Mn[d]	5.88841	—	0.566168	FM
Mg[g]-Mn	3.17440	111.2324	0.579357	FM
Mg[g]-Mn	3.23021	108.3730	0.330742	FM
Mg-Zn	3.17289	170.9862	−2.5E-5	AFM
Mn-Zn	3.38378	117.7894	0.06064	FM
Zn-Zn	5.21290, 3.157375	175.9059	−3.78329E-05, ~0	AFM

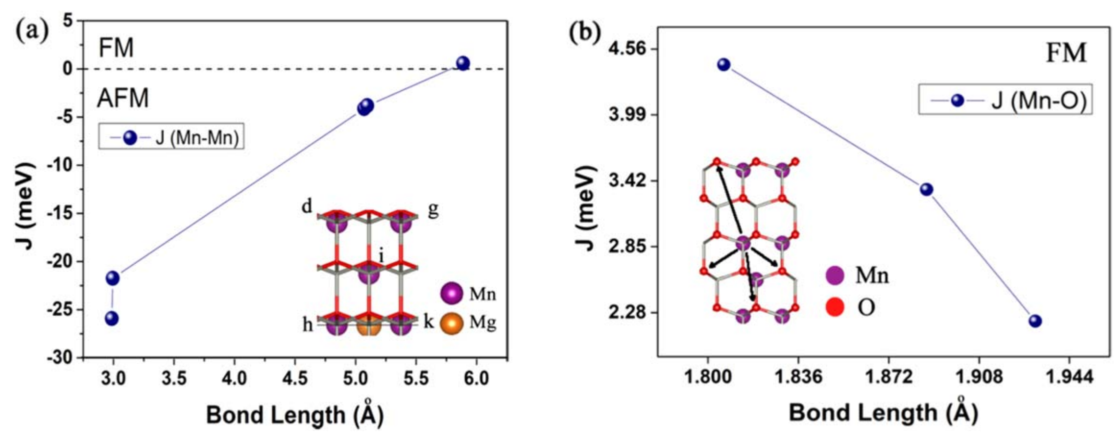

Figure 5. J values versus bond lengths of (a) Mn-Mn pairs (b) Mn-O pairs.

as −21.76 meV and −25.93 meV, respectively while 5.09671 Å and 5.07144 Å distant pairs interacted antiferromagnetically with energies of −3.82155 meV and −4.12166 meV. In contrast to the former, furthest distance of Mn-Mn pairs as 5.88841 Å contributed to FM behavior even if it is weak; herewith Mg-Mn pairs possess approximately the same sign and strength. However, Mn-O (count 4 times for an Mn) pairs showed FM behavior almost approximately 10 times of furthest distance of Mn-Mn pairs. Exchange energy of Mn-O pairs very weakened after 3 Å so they could not significantly contribute to the overall FM as can be seen in figure 5(b). Distant dependent variations of exchange coupling J corresponding to Mn-Mn and Mn-O pairs were shown in figures 5(a), (b), respectively.

The bond length of Mg-Mn neighboring oxygen couple is evidently longer than Mg-Zn neighboring oxygen couple and AFM interaction exists between Mg-O even Mn mediated a more energetic exchange value relative to Zn. However, Mn-O has an FM type interaction whose strength decreases in direct proportion with increasing distance between these atoms. FM interaction shows dominancy against AFM(10 times larger) when only MgO and MnO couples are compared. On the other hand, when the bond angle of Mn-O-Mn was increased, AFM interaction weakened up to nearly 7 times except fordistant Mn ions in which FM interaction exists. However, magnetic strengths of Mg-Mn couples were found to be high as distant Mn-Mn pairs. Mg which was bonded to Zn oxygen (Mg-O^{b,c}) and Mg-Zn, slightly contributed to the exchange mechanism of the whole system as AFM and FM state, respectively.

The intriguing nature of DMS materials, which are constructed by doping 3d or 4f TM elements forming impurities or pioneering vacancies, provided many question marks about the origin of magnetism. Several models such as p-d hybridization, superexchange, double exchange, Zener-RKKY, were suggested to make clear the origin of ferromagnetism, especially in TM doped semiconductors [1, 69–72] including nanowires [73, 74].

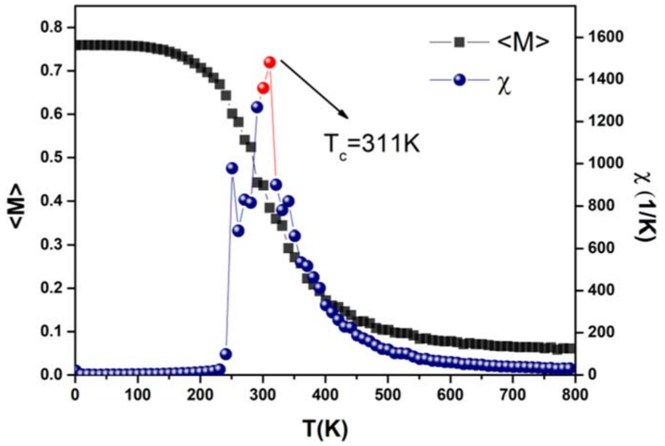

Figure 6. Black squares represent magnetization (M), and blue spheres were used to illustrate magnetic susceptibility (χ) where red spheres point the Curie temperature and the nearest temperature to the Curie temperature (left-sided), respectively, of C1 states of 5% Mn and 1%Mg-doped ZnO.

Mn-O-Mn favored strongly (relative to Zn-O-Zn) AFM due to superexchange interaction in contrast to distant Mn-Mn pairs which directly interacted through FM. In MnO case, O(p)-Mn(d) hybridization lead pairs to make an FM contribution to the system; herewith, Zn-O-Zn showed weak AFM (Zn-Zn in table 4). The abovementioned interactions commonly formed the magnetic behavior of the system, FM was preferred; however, several magnetic states exactly existed in the same system.

In the light of obtained magnetic moment (μ_B) and exchange couplings (J) from DFT, magnetic susceptibility (to determine T_c) of nanoparticles which are built on geometry optimized ZnMgMnO supercell, were calculated via Markov Chain Monte Carlo (MCMC) methods based on the Metropolis algorithm detailed in Duru *et al* [41]. Thus, transition temperature as a primary parameter for the application of magnetic materials in the device world, namely daily life, was determined by Heisenberg Hamiltonian expressed in equation (2).

$$\mathcal{H} = -\sum J_{ij}(r_{ij})\mathbf{S}_i\mathbf{S}_j - B\sum S_i^z \quad (2)$$

where S_i and S_j represent the nearest neighboring spins interacting with each other with $J_{ij}(r_{ij})$ exchange energy and B is the applied field. $|\mathbf{S}_\alpha|$was set to 1 and calculated J values (calculated by MFT) were used during the simulation. The thermal equilibrium process took 40% of total MC steps and elapsed time for expectation values was 60% at temperature (T). As shown in figure 6, magnetization versus temperature (M-T) and susceptibility measurements were taken starting from 1 K to 800 K andthe Curie temperature of $Zn_{0.94}Mg_{0.01}Mn_{0.05}O$ was found as 311 K, and it is a meaningful value, which is close to room temperature. It is obvious that nanoparticle shows FM behavior directly related to calculated exchange couplings between site atoms below 311 K. Note that distant Mn-Mn pairs (>5.8) contributed to FM while AFM behavior started to show up when they come closer. Thus, relatively big nanoparticles would possess FM like behavior in contrast to slightly small ones. Note that, in a previous study, a non-linear intriguing relation between size and magnetic behavior was found [41]. Mg-O pairs contributed to AFM state whereas Mg-Mn pairs interacted FM. This was the reason that why clustered Mg with Mn structure (C1) was preferred to be in FM state.

3. Conclusion

The structural and magnetic properties of Mg/Mn-doped ZnO were investigated by the first-principles study and Monte Carlo methods (MCs). Applying magnetic force theorem (MFT) and using Kohn-Sham orbitals in the GGA-PBE scheme, the exchange coupling parameters (J) were calculated to figure out the magnetic interactions between atomic sites one by one. According to geometry optimization of four different configurations as surface/volume clustered Mn and clustered/non-clustered Mg, Mg-Mn, Mn-Zn, Mn-O, Mg-O, Mg-Zn, Zn-Zn and O-O nearest neighbors came closer except Mn-Mn in Mg clustered structure.

Closest Mn-Mn pairsshowed strong AFM (bond length <3Å) where increasing bond angle and bond length reduced it in contrast to distant Mn ions which were interacted ferromagnetically. Mg-Mn and Mg-Zn pairs not only exhibited FM behavior but also contributed to stabilized ferromagnetism instead of being distant to Mn ions because of the AFM tendency of Mg-O pairs. MnO was strongly ferromagnetic than Mg-Mn. Magnetic behavior of $Zn_{0.94}Mg_{0.01}Mn_{0.05}O$ was designated by Mn(d)-O(p) hybridization (FM), Mn-O-Mn superexchange (AFM), and Mn-Mn direct exchange (FM) mechanisms. Calculated J values were used to determine T_c of Mg/Mn-doped ZnO nanoparticle via measuring averaged magnetization and magnetic susceptibility. The Curie temperature T_c was found as 311 K, which is absolutely above the room temperature.

Acknowledgments

Computing resources used in this work were provided by the National Center for High Performance Computing of Istanbul Technical University, (UHeM), Turkey, under grant number1006342019, the Research Fund of Bahcesehir University (BAU-BAP.2018.02.16), Istanbul, Turkey and the Scientific and Technical Research Council of Turkey (TUBITAK) through the Project No: 115F472.

ORCID iDs

I P Duru https://orcid.org/0000-0002-9227-2497
E Ozugurlu https://orcid.org/0000-0002-1301-6963
L Arda https://orcid.org/0000-0003-0722-3891

References

[1] Sato K and Katayama-Yoshida H 2002 Physics, *ab initio* study on the magnetism in ZnO-, ZnS-, ZnSe- and ZnTe- based diluted magnetic semiconductors *Phys. Status Solidi* B **229** 673
[2] Wang Z L 2004 Zinc oxide nanostructures: growth, properties, and applications *J. Phys. Condens. Matter* **16** R829
[3] Pearton S J, Norton D P, Ip K, Heo Y W and Steiner T 2005 Recent progress in processing and properties of ZnO *Prog. Mater Sci.* **50** 293–340
[4] Özgür Ü, Alivov Y I, Liu C, Teke A, Reshchikov M, Doğan S, Avrutin V, Cho S-J and Morkoc H 2005 A comprehensive review of ZnO materials and devices *J. Appl. Phys.* **98** 11
[5] Tsukazaki A *et al* 2005 Repeated temperature modulation epitaxy for p-type doping and light-emitting diode based on ZnO *Nat. Mater.* **4** 42
[6] Huang J, Yin Z and Zheng Q 2011 Applications of ZnO in organic and hybrid solar cells *Energy Environ. Sci.* **4** 3861–77
[7] Lu M P, Lu M Y and Chen L J 2012 p-Type ZnO nanowires: From synthesis to nanoenergy *Nano Energy* **1** 247–58
[8] Guo H Y, Zhao Y, Lu N, Kan E, Zeng X C, Wu X J and Yang J L 2012 Tunable magnetism in a nonmetal-substituted ZnO monolayer: a first-principles study *J. Phys. Chem.* C **116** 11336
[9] Kołodziejczak-Radzimska A and Jesionowski T 2014 Zinc oxide— from synthesis to application: a review *Materials MDPI* **7** 2833–81
[10] Shinde K P, Pawar R C, Sinha B B, Kim H S, Oh S S and Chung K C 2014 Study of effect of planetary ball milling on ZnO nanopowder synthesized by co-precipitation *J. Alloys Compd.* **617** 404–7
[11] Khalid M, Riaz S and Naseem S 2015 Tailoring of the band gap in transition metal-doped ZnO: first principle calculations *Materials Today: Proceedings* **2** (10, Part B) 5246–50
[12] Fedorov A S, Visotin M A, Kholtobina A S, Kuzubov A A, Mikhaleva N S and Hsu H S 2017 Investigation of intrinsic defect magnetic properties in wurtzite ZnO materials *J. Magn. Magn. Mater.* **440** 5–9
[13] Kegel J, Povey I M and Pemble M E 2018 Zinc oxide for solar water splitting: a brief review of the material's challenges and associated opportunities *Nano Energy* **54** 409–28
[14] Mamamouni N, Vijaya J J, Benyoussef A, Kenz A E and Bououdina M 2018 Electronic structure and magnetic studies of V-doped ZnO: ab initio and experimental investigations *Bull. Mater. Sci.* **41** 87
[15] Sun Y, Zong Y, Feng J, Li X, Yan F, Lan Y, Zhang L, Ren Z and Zheng X 2018 Oxygen vacancies driven size-dependent d0 room temperature ferromagnetism in well-dispersed dopant-free ZnO nanoparticles and density functional theory calculation *J. Alloys Compd.* **739** 1080–8
[16] Wu J, Long F, Tang B and Tang X 2018 Electronic structure and ferromagnetic propertiesof Zn vacancies in ZnO screw dislocations: First-principles calculations *AIP Adv.* **8** 065115
[17] Arda L 2019 The effects of Tb doped ZnO nanorod: an EPR study *J. Mag. Mag. Mater.* **475** 493
[18] Sui Y R, Yue Y G, Song Y P, Yao B, Cao Y, Lang J H, Li X Y and Yang J H 2015 Cd composition induced effects on structure, optical and electrical properties of sputtered Zn1-xCdxO films *Ceram. Int.* **4** 5414
[19] Akcan D, Gungor A and Arda L 2018 Structural and optical properties of Na-doped ZnO films *J. Mol. Struct.* **1161** 299
[20] Lu J G, Ye Z Z, Zeng Y J, Zhu L P, Wang L, Yuan J and Liang Q L 2006 Structural, optical, and electrical properties of (Zn,Al)O films over a wide range of compositions *J. Appl. Phys.* **100** 073714
[21] Wolf S A, Awschalom D, Buhrman R A, Daughton J M, Molnar S V, Roukes M L, Chtchelkanova A Y and Treger D M 2001 Spintronics: a spin-based electronics vision for the future *Science* **294** 1488
[22] Ammaih Y, Abderrazak A, Hartiti B, Ridah A, Thevenin P and Siadat M 2014 Structural, optical and electrical properties of ZnO:Al thin films for optoelectronic applications *Opt. Quant. Electron.* **46** 229 - 234
[23] Cao H, Lu P, Cai N, Zhang X, Yu Z, Gao T and Wang S 2014 First-principles study on electronic and magnetic properties of (Mn, Fe)-codoped ZnO *J. Mag. Mag. Mater.* **352** 66
[24] Rezkallah I D, Koç M M, Erkovanc M, Yu Chumakov D and Chemam F 2017 Investigation of the electronic and magnetic properties of Mn-doped ZnO using the FP-LAPW method *Chin. J. Phys.* **55** 1432–40
[25] El Haimeur A, El Gana L, Addou M and El Kenz A 2018 Effect of tuning the structure on the optical and magnetic properties by various transition metal doping in ZnO/TM (TM = Fe, FeCo, Cr, and Mn) thin films *J. Supercond. Nov. Magn.* **31** 569–76
[26] Xue S, Zhang F, Zhang S, Wang X and Shao T 2018 Electronic and magnetic properties of Ni-doped zinc-blende ZnO: a first-principles study *Nanomaterials* **8** 281
[27] Liu Z, Yuan X and Yang P 2018 Investigation on electronic and magnetic properties of Co and Mn in ZnO with different doping types *J. Magn. Magn. Mater.* **461** 1–5

[28] Gallegos M V, Luna C R, Peluso M A, Damonte L C, Sambeth J E and Jasen P V 2019 Effect of Mn in ZnO using DFT calculations: magnetic and electronic changes *J. Alloys Compd.* **795** 254–60
[29] Goumrhar F, Arybou O, Salmani E, Bahmad L, Ez-Zahraouy H and Benyoussef A 2019 Magnetic properties of carbon co-doped (Zn, Mn)O using LDA and LDA-SIC approximations *J. Supercond. Novel Magn.* **32** 2275–81
[30] Tan C L, Sun D, Tian X H and Huang Y W 2016 Tuning electronic structure and optical properties of ZnO monolayer by Cd doping *Ceram. Int.* **42** 10997–1002
[31] Ohtomo A, Kawasaki M, Koida T, Masubuchi K, Koinuma H, Sakurai Y, Yoshida Y, Yasuda T and Segawa Y 1998 MgxZn1-xO as a II–VI widegap semiconductor alloy *Appl. Phys. Lett.* **72** 2466
[32] Chen N B, Wu H Z, Qiu D J, Xu T N, Chen J and Shen W Z 2004 Temperature-dependent optical properties of hexagonal and cubic MgxZn1-xO thin-film alloys *J. Phys. Condens. Matter* **16** 2973
[33] Singh J P and Chae K H 2019 Local electronic structure perspectives of nanoparticle growth: the case of MgO *ACS Omega* **4** 7140–50
[34] Chen H, Tan C, Sun D, Zhao W, Tian X and Huang Y 2018 Ultrawide range tuning of direct band gap in MgZnO monolayer via electric field effect *RSC Adv.* **8** 1392–7
[35] Ozaki T. *et al* 2016 User's manual of OpenMX Ver. 3.8 (http://openmx-square.org/openmx_man3.8/openmx3.8.pdf)
[36] Öner Y and Aktaş B 1990 Magnetization measurements and computer simulations for the magnetic hysteresis losses of reentrant Ni100-xMnxPt and Ni-Mn alloys *Phys. Rev.* B **42** 2425
[37] Liu S-R, Zhai H-J and Wang L-S 2002 s-d hybridization and evolution of the electronic and magnetic properties in small Co and Ni clusters *Phys. Rev.* B **65** 113401
[38] El-Hilo M, Dakhel A A and Ali-Mohamed A Y 2009 Room temperature ferromagnetism in nanocrystalline Ni-doped ZnO synthesized by co-precipitation *J. Magn. Magn. Mater.* **321** 2279–83
[39] Arda L, Açıkgöz M and Güngör A 2012 Magnetic and microstructure properties of ni-doped ZnO films and powder by sol-gel process *J. Supercond. Novel Magn.* **25** 2701–5
[40] Boyraz C, Doğan N and Arda L 2017 Microstructure and magnetic behavior of (Mg/Ni) co-doped ZnO nanoparticles *Ceram. Int.* **43** 15986–91
[41] Duru I P, Ozugurlu E and Arda L 2019 Size effect on magnetic properties of $Zn_{0.95-x}Mg_xNi_{0.05}O$ nanoparticles by Monte Carlo simulation *Ceram. Int.* **45** 5259–65
[42] Lichtenstein A I, Katsnelson M I and Gubanov V A 1984 Exchange interactions and spin-wave stiffness in ferromagnetic metals *J. Phys. F: Met. Phys.* **14** L125
[43] Lichtenstein, Katsnelson M I, Antropov V P and Gubanov V A 1987 Local spin density functional approach to the theory of exchange interactions in ferromagnetic metals and alloys *J. Magn. Magn. Mater.* **67** 65–74
[44] Antropov V P, Katsnelson M I, Harmon B N, vanSchilfgaarde M and Kusnezov D 1996 Spin dynamics in magnets: equation of motion and finite temperature effects *Phys. Rev.* B **54** 1019
[45] Antropov V P, Katsnelson M I and Lichtenstein A I 1997 Exchange interactions in magnets *Physica* B **336** 237–8
[46] Straumal B B, Mazilkin A A, Protasova S G, Myatiev A A, Straumal P B, Schütz G, van Aken P A, Goering E and Baretzky B 2009 Magnetization study of nano grained pure and Mn-doped ZnO films: formation of a ferromagnetic grain-boundary foam *Phys. Rev.* B **79** 205206
[47] Stashans A and Rivera K 2016 Electronic and magnetic properties of Co- and Mn-codoped ZnO by density functional theory *Chin. Phys. Lett.* **33** 097102
[48] Taib M F M, Mustaffa D T, Hussin N H, Samat M H, Ali A M M, Hassan O H and Yahya M Z A 2019 First principles study on Zn doped MgO using Hubbard U correction *Mater. Res. Express* **6** 2053–1591
[49] Duru I P, Değer C, Kalayci T and Arucu M 2015 A computational study on magnetic effects of Zn1−xCrxO type diluted magnetic semiconductor *J. Magn. Magn. Mater.* **396** 268–74
[50] Lamhal K, Hayn R, Boukortt A, Meskine S, Abbes L and Zaoui A 2018 Effect of (Co, N) co-doping of p-type ZnO on electronic and magnetic properties by DFT + U studies *Physica* B **545** 491–7
[51] Ozaki T 2003 Variationally optimized atomic orbitals for large-scale electronic structures *Phys. Rev.* B **67** 155108
[52] Ozaki T and Kino H 2004 Numerical atomic basis orbitals from H to Kr *Phys. Rev.* B **69** 195113
[53] Ozaki T and Kino H 2005 Efficient projector expansion for the ab initio LCAO method *Phys. Rev.* B **72** 045121
[54] Lejaeghere K *et al* 2016 Reproducibility in density functional theory calculations of solids *Science* **351** aad3000
[55] Perdew J P, Burke K and Ernzerhof M 1996 Generalized gradient approximation made simple *Phys. Rev. Lett.* **77** 3865
[56] Monkhorst H J and Pack J D 1976 Special points for Brillouin-zone integrations *Phys. Rev.* B **13** 5188–92
[57] Yoon H, Kim T J, Sim J H, Jang S W, Ozaki T and Han M J 2018 Reliability and applicability of magnetic-force linear response theory: numerical parameters, predictability, and orbital resolution *Phys. Rev.* B **97** 125132
[58] Zeng Z, Guenzburger D and Ellis D E 1999 Electronic structure, spin couplings, and hyperfine properties of nanoscale molecular magnets *Phys. Rev.* B **59** 6927
[59] Boukhvalov D W, Lichtenstein A I, Dobrovitski V V, Katsnelson M I, Harmon B N, Mazurenko V V and Anisimov V I 2002 Effect of local Coulomb interactions on the electronic structure and exchange interactions in Mn12magnetic molecules *Phys. Rev.* B **65** 184435
[60] Boukhvalov D W, Dobrovitski V V, Katsnelson M I, Lichtenstein A I, Harmon B N and Kögerler P 2003 Electronic structure and exchange interactions in V15 magnetic molecules: LDA + U results *J. Appl. Phys.* **93** 7080
[61] Boukhvalov D W *et al* 2003 Electronic structure of magnetic molecules V15: LSDA + U calculations, x-ray emissions, and photoelectron spectra *Phys. Rev.* B **67** 134408
[62] Dobrovitski V V and De Raedt H A 2003 Efficient scheme for numerical simulations of the spin-bath decoherence *Phys. Rev.* E **67** 056702
[63] Han M J, Ozaki T and Yu J 2004 Electronic structure, magnetic interactions, and the role of ligands in Mnn (n = 4, 12) single-molecule magnets *Phys. Rev.* B **70** 184421
[64] Heiba Z K and Arda L 2009 Structural properties of $Zn_{1-x}Mg_xO$ nanomaterials prepared by sol-gel method *Cryst. Res. Technol.* **44** 845
[65] Goodenough J B 1958 An interpretation of the magnetic properties of the perovskite-type mixed crystals $La_{1-x}Sr_xCoO_{3-\lambda}$ *J. Phys. Chem. Solids* **6** 287–97
[66] Kanamori J 1959 Superexchange interaction and symmetry properties of electron orbitals *J. Phys. Chem. Solids* **10** 87–98
[67] Anderson P W 1950 Antiferromagnetism. Theory of superexchange interaction *Phys. Rev.* **79** 350–6
[68] Ahmad T, Khatoon S and Al-Hartomy O A 2017 Solvothermal synthesis of $Zn_{1-x}Mn_xO$ nanoparticles using oxalate precursor route: optical and magnetic properties *Arabian J. Chem.* **10** S2138–44
[69] Akai H 1998 Ferromagnetism and its stability in the diluted magnetic semiconductor (In, Mn) As *Phys. Rev. Lett.* **81** 3002

[70] Dietl T, Ohno H, Matsukura F, Cibert J and Ferrand D 2000 Zener model description of ferromagnetism in zinc-blende magnetic semiconductors *Sience* **287** 1019

[71] Devi A A S and Roqan I S 2016 The origin of room temperature ferromagnetism mediated by Co–VZn complexes in the ZnO grain boundary *RSC Adv.* **6** 50818–24

[72] Tian Y *et al* 2011 Bound magnetic polarons and p-d exchange interaction in ferromagnetic insulating Cu-doped ZnO *Appl. Phys. Lett.* **98** 162503

[73] Devi A A S, Schwingenschlögl U and Roqan I S 2014 Ferromagnetism in Gd doped ZnO nanowires: a first principles study *J. Appl. Phys.* **116** 233906

[74] Devi A A S and Roqan I S 2015 Defect-impurity complex induced long-range ferromagnetism in GaN nanowires *Mater. Res. Express* **2** 126104

[75] Senol S D, Guler A, Boyraz C and Arda L 2019 Preparation structure and magnetic properties of Mn-Doped ZnO nanoparticles prepared by hydrothermal method *J. Supercond. Novel Magn.* **32** 2781–86